Title: *Experimental identification of structural dynamics and aeroelastic properties of a self-sensing smart composite wing*

Proceedings of the 10th International Workshop on Structural Health Monitoring 2015

Authors: Fotis Kopsaftopoulos
Raphael Nardari
Yu-Hung Li
Pengchuan Wang
Bo Ye
Fu-Kuo Chang

in the Proceedings of the 10th International Workshop on Structural Health Monitoring
September 2015, Stanford, CA, USA

ABSTRACT

Self-sensing intelligent composite materials with state-sensing and awareness capabilities constitute the future of aerospace structures. The objective of this work is to develop technologies that will lead to the next generation of intelligent aerospace structures that can sense the environmental conditions and structural state, effectively interpret the sensing data to achieve real-time state awareness, and employ appropriate self-diagnostics under varying operational environments. In this paper, the design, integration, and experimental identification of the structural dynamics and aeroelastic properties are presented for an intelligent composite UAV wing. Bio-inspired stretchable sensor networks, including integrated piezoelectric, strain, and temperature sensors are monolithically embedded in the composite layup to provide the sensing capabilities. Stochastic signal processing and identification techniques are employed in order to accurately interpret the sensing. The experimental evaluation and assessment is demonstrated via a series of wind tunnel experiment under varying angles of attack and airflow velocities for the identification of the coupled airflow-structural dynamics and strain distribution. The obtained results demonstrate the successful integration of the micro-fabricated stretchable sensor networks with the composite wing, as well as the effectiveness of the stochastic data interpretation approaches. This study constitutes a significant step in proving the integration potential of the approach for the next generation of fly-by-feel UAVs.

INTRODUCTION

Future intelligent autonomous vehicles will be able to “feel”, “think”, and “react” in real time enabling high-resolution state-sensing, awareness, and self-diagnostic capabilities. They will be able to sense and observe phenomena at unprecedented length and time scales allowing for superior performance in complex dynamic environments, safer operation, reduced maintenance costs, and complete life-cycle

---

F. Kopsaftopoulos, R. Nardari, Y.-H. Li, P. Wang, F.-K. Chang, Department of Aeronautics and Astronautics, Stanford University, Stanford, CA, U.S.A..

Bo Ye, Faculty of Electric Power Engineering, Kunming University of Science and Technology, Kunming, China.

management. Despite the importance of vehicle state sensing and awareness, however, the current state of the art is primitive as well as prohibitively heavy, expensive, and complex. Therefore, a departure from the existing technologies is necessary for the design and deployment of the next generation of aerospace structures.

The use of composite materials in aerospace structures is increasing due to their superior properties of strength, stiffness, weight, performance, and corrosion resistance. A dramatic rise is seen in the application of advanced composite materials for aerospace applications in the last two decades. Industry analysts estimate a growth of 8-13% per year in the carbon fiber reinforced plastics market for the next several years [1]. The increased use of composites and the desire to sense the environment, improve the performance, increase the safety, and enable condition-based maintenance based on structural health monitoring (SHM) techniques necessitates the integration of real-time state sensing and awareness capabilities [2-4].

Self-sensing multifunctional materials are highly "intelligent" materials that constitute the future generation of composites for aerospace applications [5-7]. Towards this end, current research aims at the development of the technologies that will lead to the next generation of autonomous aerospace systems that can sense the environment (temperature, pressure, humidity, etc.) and structural state (configuration, loads, damage, etc.), and effectively interpret the sensing data to achieve real-time state awareness under uncertainties in varying operating environments. Such self-sensing composite materials will enable the integration with SHM systems [8-13] in which a network of sensors is attached or embedded inside the composite structure.

In this work, the complete design, integration, and wind tunnel experimental assessment are presented for an intelligent composite UAV wing with state-sensing and awareness capabilities. The proposed incorporates novel bio-inspired multi-modal sensor networks that can be embedded inside composite materials to provide built-in sensing and intelligence capabilities to various structural components (wings, fuselage, other critical components). Micro-fabricated stretchable sensor networks, including integrated piezoelectric, strain, and temperature sensors are designed and monolithically embedded in the layup of the composite wing. In addition, stochastic signal processing and system identification techniques are employed in order to accurately interpret the sensing data collected from piezoelectric and strain sensors. The experimental evaluation and assessment of the intelligent wing is demonstrated via wind tunnel experiments under varying angles of attack and airflow velocities for the identification of the coupled airflow-structural dynamics and the investigation of the strain distribution for the considered operating conditions.

PROBLEM STATEMENT AND METHOD OF APPROACH

The objective of this work is to demonstrate the design, integration and experimental assessment of an intelligent composite UAV wing outfitted with four stretchable sensor networks that are embedded inside the carbon/glass fiber composite layup. The schematic representation of the proposed bio-inspired UAV concept is presented in Figure 1.

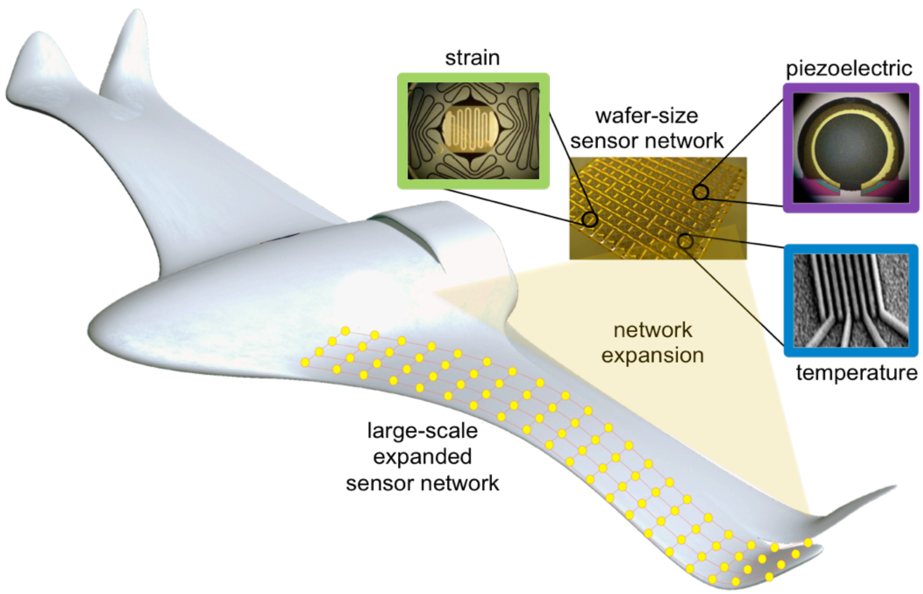

Figure 1: Schematic representation of the intelligent UAV wing concept with bio-inspired multi-modal stretchable sensor networks embedded inside the composite structural components.

Each of the four sensor networks fabricated for this work consist of 8 piezoelectric lead-zirconate titanate (PZT) sensors, 6 strain gauges, and 23 resistive temperature detectors (RTDs). The fabricated wing can sense its structural state and surrounding environment during flight and interpret the sensing information in order to determine its actual operating state and flight configuration. Piezoelectric sensors are used to sense the vibration of the wing in order to identify the coupled airflow-structural dynamics. Strain gauges are used to determine the strain distribution of the wing and identify potential critical areas for the considered experimental conditions. Wind tunnel experiments were conducted for various angles of attacks and freesrteam airflow velocities for the investigation of a broad regime of flight conditions and structural states.

The method of approach is divided into three major tasks: (i) bio-inspired multi-modal stretchable sensor networks for state sensing; (ii) wing structural design and fabrication via integrated sensor networks and composite materials; (iii) state awareness via statistical signal processing and stochastic identification techniques for data processing and interpretation.

BIO-INSPIRED STRETCHABLE SENSOR NETWORKS

The Structures and Composites Laboratory (SACL) at Stanford University has spent a significant amount of effort in the past decade on state-of-the-art research related to bio-inspired sensor technologies, stretchable sensor networks, and microfabrication techniques [5-7,14-17]. The SACL has significant experience in developing sensor networks for structural sensing applications and SHM. To address large-scale composites monitoring issues micro-fabricated expandable sensor networks are developed via the use of nonstandard C-MOS and MEMS processes to mass fabricate integrated networks of sensors that can be installed monolithically.

Recently microfabricated expandable sensor networks have been developed and deployed micro-scale sensors over macroscopic areas [5-7,14-17]. In order to survive the large strains that occur in expansion, the sensors are created on polymer substrates with nonstandard and unique microfabrication processes. The resulting components have dimensions on the order of tens of micrometers (Figure 2).

These networks are created on standard 100 mm diameter substrates and expanded to span areas orders of magnitude larger than the initial fabrication area deploying numerous micro-meter scale devices over meter scale areas. The resulting web-like network consists of distributed small scale components (nodes, wires, pads, etc.) intended to have a minimal parasitic effect on the host structure. The component size is on the same order as an individual fiber in typical composite materials or scrim in film adhesives and small enough to be placed into a composite without structural modifications. These networks can be used in-situ, from the material fabrication throughout its service life, to monitor the cure process of composite materials, characterize material properties post-cure, and monitor the structural dynamics along with the health of the structure during its life cycle.

In this work four stretchable sensor networks with integrated distributed PZT, strain, and RTD sensors have been designed and fabricated [14-17] so that they can be embedded inside the composite layup of the intelligent wing. Extensible wires connect the network nodes and serve as the signal communication channels. Before stretching, the network dimensions are 52.8 mm by 39.6 mm that after the stretching process expand to 140 mm by 105 mm yielding a 700% total surface area increase [17]. Each of the four sensor networks contains 8 piezoelectric sensors (round PZTs ⅛ in diameter), 6 strain gauges, and 24 RTDs. The total number of embedded sensors in the composite wing is 148.

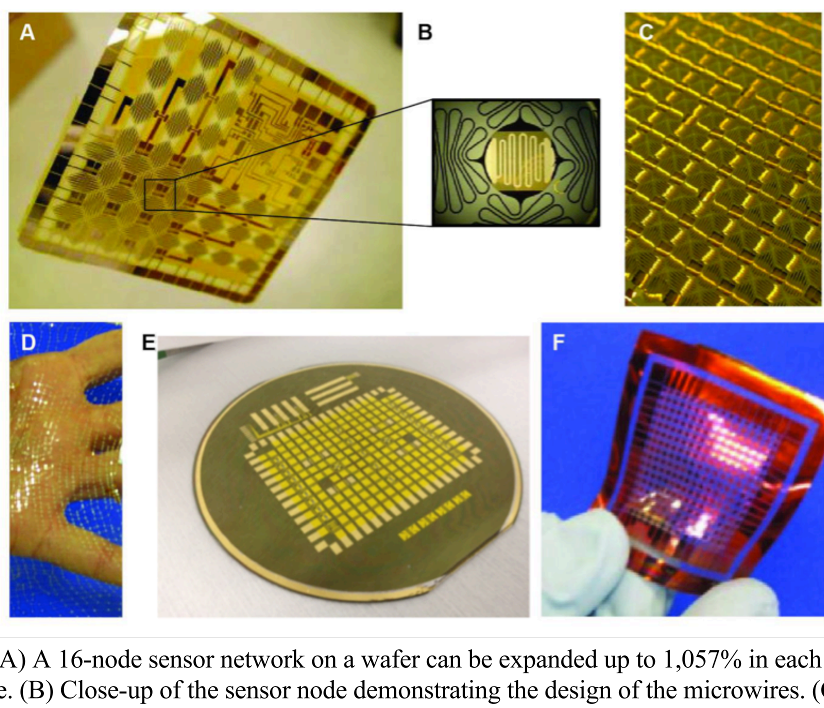

Figure 2: (A) A 16-node sensor network on a wafer can be expanded up to 1,057% in each dimension after release. (B) Close-up of the sensor node demonstrating the design of the microwires. (C) A sensor network with 169 nodes before expansion. (D) An expanded 5041-node network is shown in contrast to a hand, which illustrates the flexibility of the membrane. (E) Network before release on a 4-inch wafer. (F) A fabricated 256-node network on polyimide is easily held by hand without damaging the network. It is characterized by 16 µm wide, 50 µm thick microwires.

THE INTELLIGENT COMPOSITE WING

The prototype intelligent composite wing was designed, constructed and tested in the wind tunnel at Stanford University. Analyzing a prototype model with construction typical of that of an operational UAV wing will allow for practical weight and performance comparison with existing systems, as well as enabling a scaling analysis. The designed wing is based on the cambered SG6043 high lift-to-drag ration airfoil with a 0.86 m wing span, 0.235 m chord, and an aspect ratio of 3.66. In order to achieve the successful integration and fabrication of the wing prototype, an appropriate network-material integration process had to be developed for embedding the micro-fabricated sensor networks inside the composite materials. Figure 3 presents the design of the intelligent composite wing prototype.

The micro-scale, aspect ratio, and fragile nature of the stretchable network components, including both the wires acting as the communication channels and the sensor nodes, requires the use of an appropriate integration and network transfer process that takes into account and effectively tackles the sensitive nature of the micro-components. Moreover, the geometry and material of the network nodes and contact pads may cause the electrical shorting with the carbon fibers if not properly addressed. In order to tackle these integration and manufacturing challenges, a new process had to be developed for the transfer, electrical interfacing and electrical insulation of the network components based on multilayers flexible PCB technologies and epoxy armor. Using the developed approach the sensor networks were successfully integrated into carbon fiber based composite materials using a multi-step fabrication process. The composite wing structure was manufactured in the form of carbon and glass laminated composites. The layup consists of carbon fiber (CF) plain wave fabric 1K T300 and glass fiber (GF) plain wave fabric 18 gr/m^2 infused using Araldite LY/HY5052 epoxy. The stacking sequence of the layers was [0º GF, 0º CF, 45º CF, 45º CF, 0º CF, 0º GF] (Figure 3).

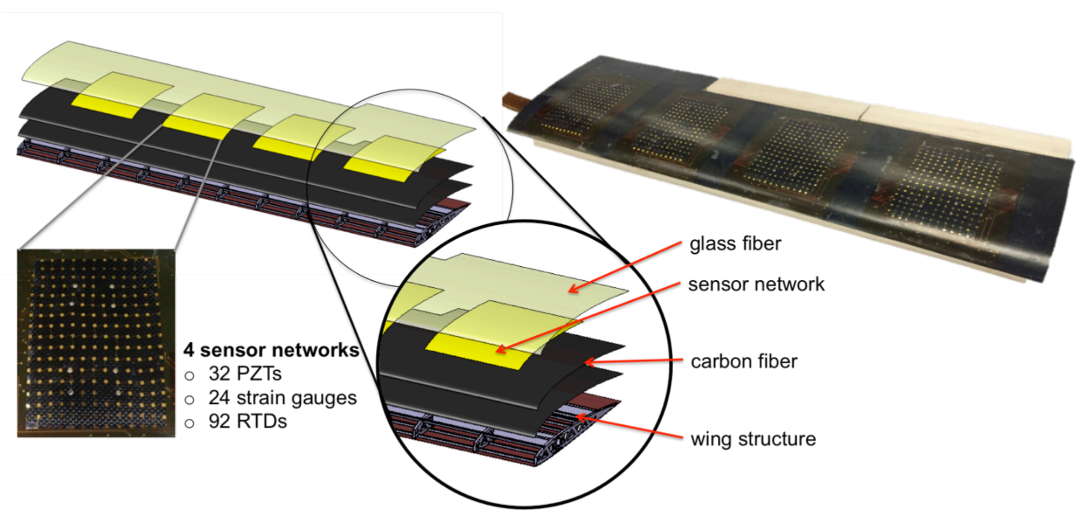

Figure 3: The intelligent composite wing design with a total of 148 (32 piezoelectric, 24 strain gauges, and 92 RTDs) micro-sensors embedded in the composite layup.

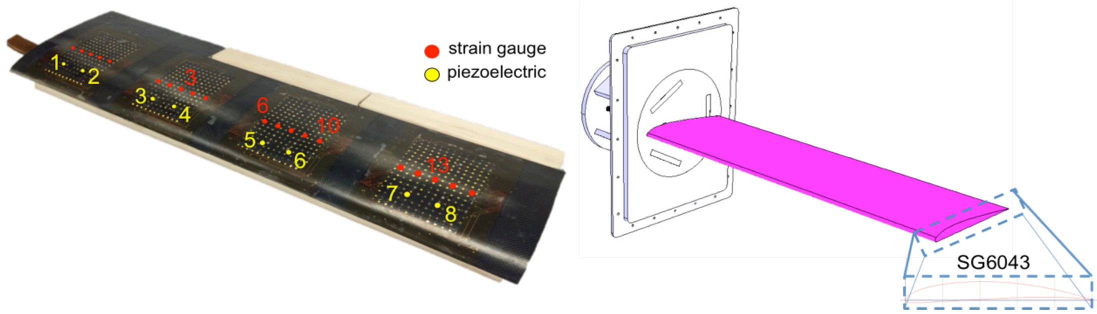

Figure 4: The intelligent composite wing with the embedded sensor networks and the locations of the piezoelectric and strain sensors.

The four networks were embedded between the two top layers at 0º of the layup (near the wing surface) during the lamination process. The glass fiber was employed due to its transparency, so that the embedded stretchable sensor networks may be evident to the naked eye. The supporting structure of the composite wing consists of wooden (basswood) ribs and spars on which the composite skin was mounted.

THE EXPERIMENTAL SETUP

Wind Tunnel

The prototype composite wing was tested in the open-loop wind tunnel (WT) facility at Stanford University. The WT has a square test section of 76 cm by 0.76 cm (30 by 30 in) and can achieve continuous flow speeds up to approximately 40 m/s. A custom basis was designed and fabricated to support the wing and permit adjustments in the angle of attack (AoA). As the wing span was slightly longer than the wind tunnel test section, an additional 10 cm (4 in) extension was attached to the wing fixture. The wing was mounted horizontally inside the test section. Eight commercial strain gauges were attached on appropriate locations of the basis to measure the aerodynamic forces. The axis of rotation coincided approximately with the quarter of the wing chord. Figure 4 presents the composite wing with the corresponding locations of the PZTs and strain sensors. TABLE I presents the wing dimensions.

The Experiments

A series of wind tunnel experiments were conducted for various AoAs and freesrteam velocities U_∞. For each AoA, from 0 degrees up to 18 degrees, data were sequentially collected for velocities from 6 m/s up to 22 m/s. The above procedure resulted in 285 different experiments covering the complete range of the considered experimental conditions (AoAs and freestream velocities). The experimental conditions along with the Reynolds numbers are outlined in TABLE II.

TABLE I. WING DIMENSIONS

chord *c*	0.235 m
span *b*	0.86 m
area *S*	0.2 m^2
aspect ratio *AR*	3.66

TABLE II. THE CONSIDERED EXPERIMENTAL CONDITIONS

Re ($\times 10^3$)	93	124	155	171	187	202	217	233	248	264	280	295	311	326	342
U_∞ (m/s)	6	8	10	11	12	13	14	15	16	17	18	19	20	12	22
Angle of attack:	0 – 18 degrees									**Total number of experiments: 285**					

TABLE III: THE SENSORS, DATA ACQUISITION, AND SIGNAL DETAILS

	PZT sensors	**Strain gauges**
Number of sensors	8	15
Sampling frequency f_s	1000 Hz	100 Hz
Sampling bandwidth	[0.5 – 200] Hz	[DC – 40] Hz
Signal length in samples (s)	90,000 (90 s)	9,000 (90 s)

For each experiment the vibration and strain responses were recorded at different locations on the wing via the embedded network PZTs (sampling frequency $f_s = 1000$ Hz, signal bandwidth 0.5–200 Hz) and strain gauges (sampling frequency $f_s = 100$ Hz, signal bandwidth DC–100 Hz), respectively. The strain signals were driven through a custom designed and built signal conditioning device into the data acquisition system (National Instruments). The total number of the sensor signals that were obtained was limited by the available number of channels of the data acquisition system. TABLE III presents the sensors, data acquisition, signal details.

NUMERICAL SIMULATIONS

In order to extract the aerodynamic properties of the fabricated wing based on which the experimental results will be interpreted and assessed, a series of numerical simulations were conducted using the XFOIL, an interactive program for the design and analysis of subsonic isolated airfoils developed at MIT [18]. Given the coordinates specifying the shape of the 2D airfoil, Reynolds number and freestream velocity XFOIL can calculate the pressure distribution on the airfoil and hence lift and drag characteristics.

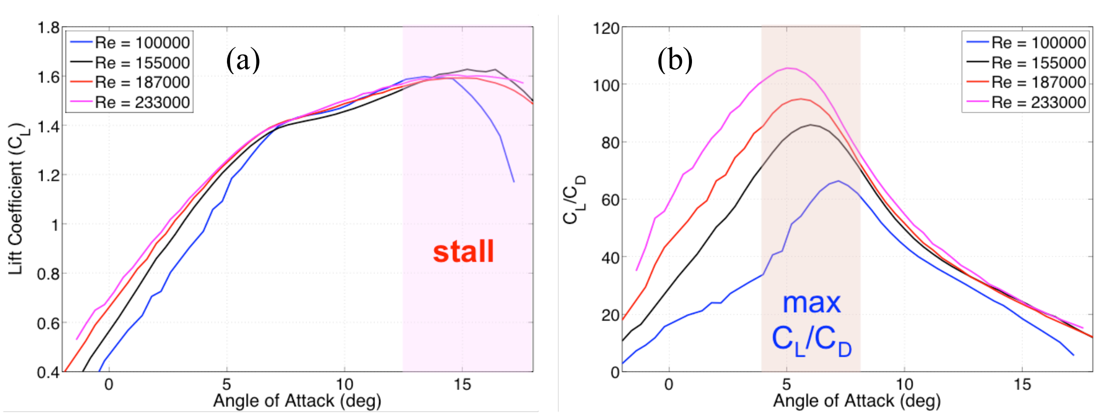

Figure 5: Indicative simulation results: (a) lift coefficient and (b) lift to drag coefficient ratio C_L/C_D versus angle of attack for the SG6043 airfoil and various Reynolds numbers.

Figure 5a and Figure 5b present the lift coefficient versus the angle of attack and lift to drag coefficient ratio C_L/C_D results of the SG6043 airfoil of the wing, respectively, for various Reynolds numbers (U_∞ = 7, 10, 12 and 15 m/s). It may be readily observed that the wing exhibits stall (loss of lift shown as shaded area in Figure 5a) starting from an angle of attack of approximately 12 degrees for a Reynolds number of Re=100,000. Moreover, observe that the maximum C_L/C_D ratio is obtained for angles between 4 and 8 degrees (shaded areas in Figure 5b).

EXPERIMENTAL RESULTS

Figure 6 presents indicative signals obtained from PZT sensor 2 (see Figure 4) under various angles of attack and a freestream velocity U_∞ = 11 m/s (Re = 171,000). Observe the random (stochastic) nature of these signals, which is due to the wind tunnel airflow actuation and the fluid-structure interaction. In addition, it is evident that for higher angles of attack and as the wing approaches stall the signal amplitude (voltage) increases. Figure 7 presents indicative signal energy (volt^2·t) results for PZT sensors 2 and 5 obtained from the wind tunnel experiments for angles between 0 and 18 degrees and freestream velocities of 11 m/s, 12 m/s, 14 m/s, and 15 m/s. The goal is to correlate the signal energy in the time domain with the airflow characteristics, the structural dynamics and aeroelastic properties in order to identify and track appropriate signal features that can be used for the airflow and wing vibration monitoring, the localization of the flow separation over the wing chord, and the early detection of stall under various flight and environmental conditions. The signal energy evolution with respect to the angle of attack is similar in both cases. As the wing angle exceeds the value of 12 degrees the signal energy significantly increases and reaches the maximum value in the stall range. Notice that for the velocities of 11 m/s and 12 m/s the stall angle is 13 degrees, whereas for the higher velocities of 14 m/s and 15 m/s the stall angle appears at 14 degrees. In both cases observe the significant increase in the signal energy that starts approximately at 11 degrees. These results are in agreement with the trend of signals in Figure 6 as in both cases the signal amplitude/energy is maximized within the stall range of the wing.

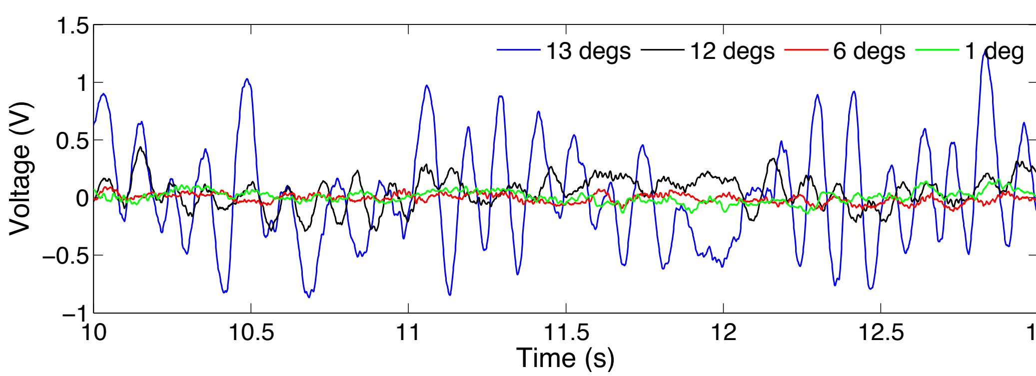

Figure 6: Indicative signals obtained from PZT sensor 2 under various angles of attack for a freestream velocity U_∞ = 11 m/s (Re = 171,000).

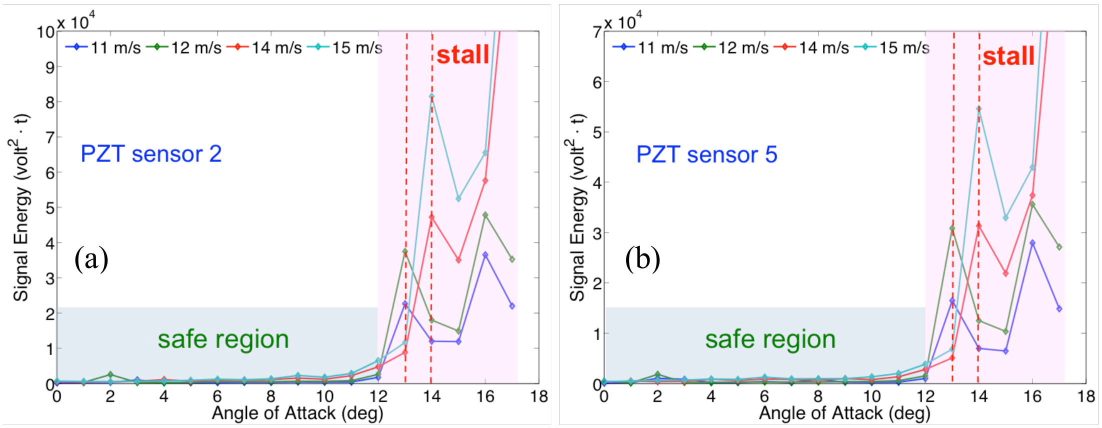

Figure 7: Indicative wind tunnel signal energy results for (a) PZT sensor 2 and (b) PZT sensor 5 under various freestream velocities. The safe and stall regions for are shown in shaded areas.

Indicative results obtained from strain gauges 3 and 10 are presented in Figure 8a and Figure 8b, respectively. The recorded strain is plotted for increasing angle of attack and airspeed (freestream velocity), hence the strain mapping for the specific location on the wing may be obtained for the considered experimental conditions. As the angle of attack and airspeed increase the applied strain also increases, with the maximum strain appearing in the top right corner of the figures. The strain shown in these plots is estimated as the mean value of the acquired signal (9000 samples; 90 s). The maximum strain is observed for angles higher than 8 degrees and velocities higher than 16 m/s, resulting in a critical, with respect to strain, flying area of the wing that for the considered experimental conditions (or –in the more general concept– flight envelope) is located in the top right corner of the figures (shown as red dashed rectangular). In addition, it may be observed that a somewhat increased strain area, shown as a blue dashed rectangular, appears between angles of 4 and 7 degrees. This area corresponds to the maximum CL/CD ratio of the wing airfoil as also presented in Figure 5. Finally, the recorded strain is higher for gauge 3 than gauge 10, as it may be concluded from Figure 8. This is due to the fact that strain gauge 3 is closer to the root of the wing, as shown in Figure 4, and thus it is expected that the quasi-static strain in that location should be higher than the strain closer to the wing tip.

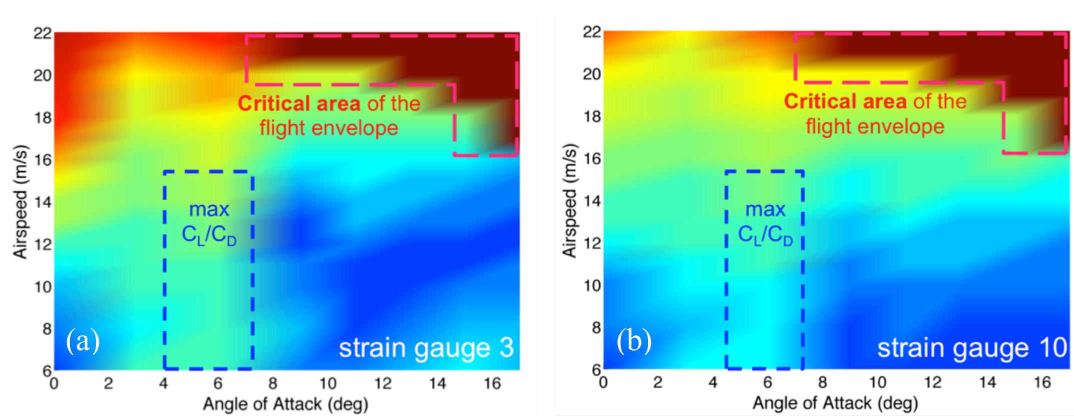

Figure 8: Indicative strain distribution obtained from (a) strain gauge 3 and (b) strain gauge 10 for the considered angles of attack and freestream velocities.

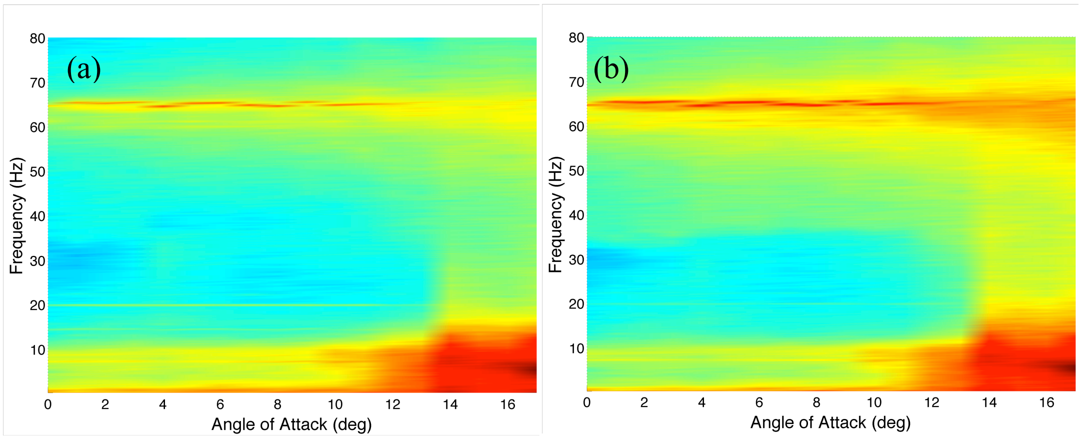

Figure 9: Indicative three-dimensional Welch-based PSD estimates (PZT sensor 5) versus angle of attack for (a) $U_\infty = 11$ m/s (Re = 171,000) and (b) $U_\infty = 15$ m/s (Re = 233,000) freestream velocities.

In addition to the time domain analysis, the signals are transformed to the frequency domain so that the spectral estimates may be explored and analyzed, and the correlation of the sensors' response with the coupled airflow-structural dynamics may be investigated. Non-parametric identification of the wing dynamics is based on N = 90000 (90 s) sample-long response signals recorded from the PZT sensors (see TABLE III). An $L = 5096$ sample-long Hamming data window (frequency resolution $\Delta f = 0.24$ Hz) with 90% overlap is used for the power spectral density (PSD) estimation via the Welch-based method.

Figure 9 presents indicative PSD Welch-based estimates of the response signals obtained from PZT sensors 2 and 5 for increasing AoA and velocity of $U_\infty = 15$ m/s (Re = 233,000). Notice that as the angle of attack increases the wing vibration PSD amplitude in the lower frequency range of [1 – 12] Hz significantly increases. More specifically, as the angle of the wing approaches the critical stall angle of 13 degrees the low frequency vibrations become dominant and thus indicating the proximity to wing stall. In this Figure it is evident that by monitoring the identified lower frequency bandwidths that are sensitive to increasing angle of attack we may have a strong indication of stall. Furthermore, by comparing Figure 9a with Figure 9b we may observe that the frequency of 66 Hz is more evident in the case of sensor 5.

Figure 10 presents indicative PSD Welch-based estimates for all the PZT sensors along the wing span axis versus the wing span axis location for a velocity of $U_\infty = 15$ m/s (Re = 233,000). Figure 10a presents the wing natural frequencies along the wing span for an AoA of 3 degrees while Figure 10b shows the corresponding results for an AoA of 13 degrees. For the latter AoA the wing is under stall condition. Notice that for the case of Figure 10b under stall condition the wing vibration as represented by the PSD amplitude is much more significant in the lower frequency range of [1 – 12] Hz when compared to an AoA of 3 degrees. Similarly, by examining this Figure it is evident that by monitoring the identified lower frequency bandwidths that are sensitive to increasing AoA we may have a strong indication of stall.

Finally, Figure 11 presents indicative PSD Welch-based estimates of the response signals obtained from PZT sensor 5 for increasing freestream velocity and angles of attack of 6 and 12 degrees. Notice that as the airspeed increases the PSD amplitude in both the lower [1 – 12] Hz and higher [40 – 80] Hz frequency ranges significantly increase. Overall, it may be observed that the lower frequency vibrations are more evident in Figure 11b that corresponds to a higher, close to stall, angle of attack, Again, it is evident that by monitoring appropriate frequency bandwidths we may have a strong indication of both the stall and airspeed flight conditions.

Due to the evident correlation of the wing natural frequencies with the angle of attack and airspeed evolution, we may conclude that the coupled airflow-structural dynamics may be identified and represented by the estimated Welch-based PSDs, thus providing an initial direct indication, along with the signal energy of Figure 7, of the loss of lift and the dynamic stall phenomenon

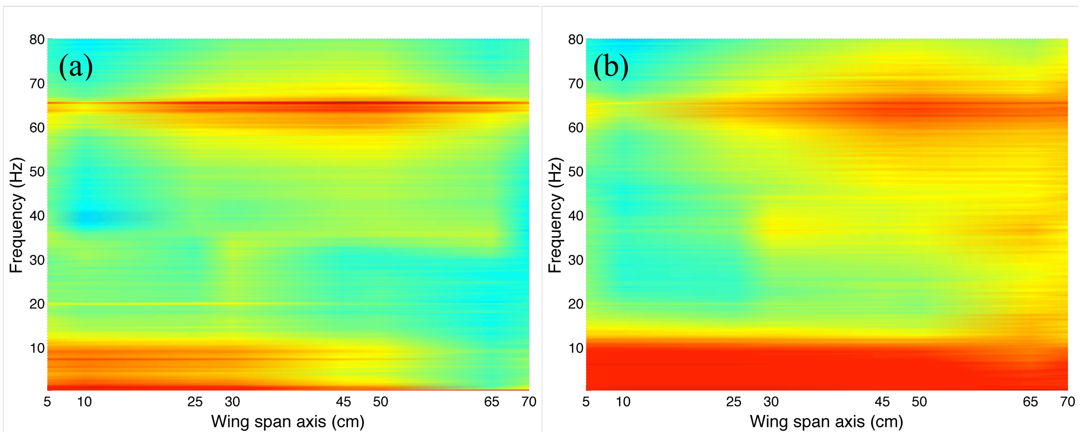

Figure 10: Indicative Welch-based PSD estimates for all the PZT sensors along the wing span versus the wing span axis for U_∞ = 15 m/s (Re = 233,000). (a) AoA of 3 degrees and (b) AoA of 13 degrees under wing stall condition.

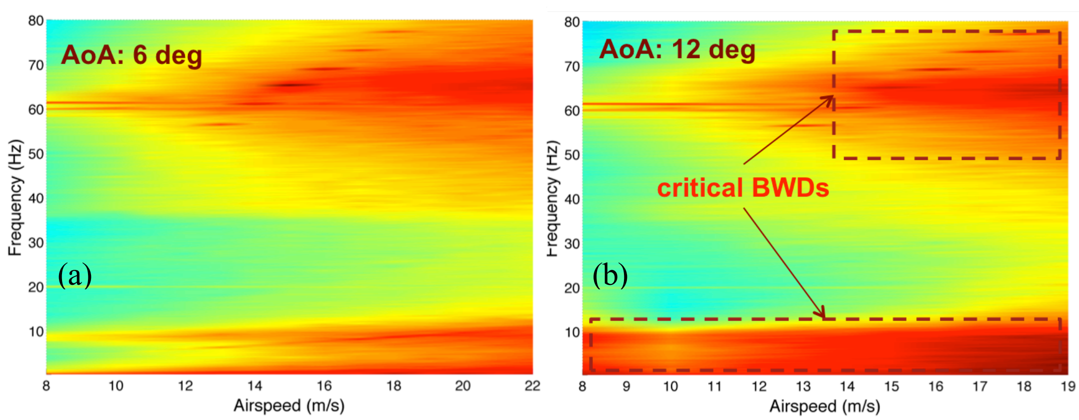

Figure 11: Indicative three-dimensional Welch-based PSD estimates (PZT sensor 5) versus airspeed for angles of attack of (a) 6 degrees (laminar flow) and (b) 12 degrees (flow separation; close to stall angle). The critical frequencies bandwidths are shown in the dashed rectangular areas.

CONCLUSIONS

The objective of this work was to experimentally demonstrate that the designed self-sensing intelligent composite UAV wing has superior state sensing and awareness capabilities when compared to the existing state-of-the-art technologies. The embedded bio-inspired stretchable sensor networks that consist of PZTs, strain gauges, and RTDs enable the identification of the coupled structural and aerodynamic properties under normal operating conditions under uncertainties. The fabricated prototype intelligent wing was able to sense its structural state and surrounding environment and interpret the sensing information in order to determine its actual operating state and flight configuration. Piezoelectric sensors were used to sense the vibration of the wing in order to identify the coupled airflow-structural dynamics, while strain gauges were used to determine the strain distribution of the wing and identify potential critical areas for the considered operating conditions. Appropriate wind tunnel experiments were conducted for various angles of attacks and freesrteam velocities for the investigation of a broad regime of flight conditions and structural states. The obtained results demonstrated the successful integration of the micro-fabricated stretchable sensor networks with the composite materials of the wing, as well as the effectiveness of the stochastic data interpretation approaches, proving their integration potential into fly-by-feel UAVs and enabling their deployment for the next generation of aerospace structures.

ACKNOWLEDGEMENTS

This research was supported by the U.S. Air Force Office of Scientific Research (AFOSR) Multidisciplinary University Research Initiative (MURI) program under grant FA9550-09-1-0677. The authors appreciate the support of Dr. Yung-Gyo Lee, Hao Dong, Huafei Wang, and the contribution of Dr. Jun Wu, Dr. Shao Bo in the experimental procedure. Finally, the authors would like to acknowledge the support of Dr. Lester Su and Prof. John Eaton in the wind tunnel facility at Stanford University.

REFERENCES

1. M. Holmes. 2014. “Global carbon fibre market remains on upward trend”, *Reinforced Plastics*, 58(6):38-45.
2. A. Harris, 2003. *Fatigue in composites*, Cambridge, England: Woodhead Publishing.
3. P. Johnson and F.-K. Chang. 2001. “Characterization of matrix crack-induced laminate failure - Part 1: Experiments”, *Journal of Composite Materials*, 35(22):2009-2035.
4. P. Beaumont, R. Dimant and H. Shercliff. 2006. “Failure processes in composite materials: getting physical”, *Journal of Material Science*, 41:6526-6546.
5. N. Salowitz, Z. Guo, S. Roy, R. Nardari, Y.-H. Li, S.-J. Kim, F. Kopsaftopoulos and F.-K. Chang. 2014. “Recent advancements and vision toward stretchable bio-inspired networks for intelligent structures”, *Structural Health Monitoring*, 13(6):609-620.
6. G. Lanzara, N. Salowitz, Z. Guo and F.-K. Chang. 2010. “A spider-web-like highly expandable sensor network for multifunctional materials”, *Advanced Materials*, 22(41):4643-4648.
7. N. Salowitz, Z. Guo, Y.-H. Li, K. Kim, G. Lanzara and F.-K. Chang. 2013. “Bio-inspired stretchable network-based intelligent composites”, *Journal of Composite Materials*, 47(1):97-106.
8. C. Larrosa, K. Lonkar and F.-K. Chang. 2014. “In situ damage classification for composite laminates using Gaussian discriminant analysis”, *Structural Health Monitoring*, 13(2):190-204.
9. J.B. Ihn and F.-K. Chang. 2004. “Detection and monitoring of hidden fatigue crack growth using a built-in piezoelectric sensor/actuator network, Part I: Diagnostics”, *Smart Materials and Structures*, 13:609-620.
10. J.B. Ihn and F.-K. Chang. 2004. “Detection and monitoring of hidden fatigue crack growth using a built-in piezoelectric sensor/actuator network, Part II: Validation through riveted joints and repair patches”, *Smart Materials and Structures*, 13:621-630.

11. J.B. Ihn and F.-K. Chang. 2008. "Pitch-catch active sensing methods in structural health monitoring for aircraft structures", *Structural Health Monitoring*, 7(1):5-19.
12. V. Janapati, K. Lonkar and F.-K. Chang. 2012. "Real time in-situ damage classification, quantification and diagnosis for composite structures", *19th International Congress on Sound and Vibration*, Vilnius, Lithuania, July 2012.
13. S. Roy, I. Mueller, V. Janapati, S. Das and F.-K. Chang. 2012. "Real-time prediction of impact-induced damage for composite structures based on failure analysis and efficient database methods", *SPIE Annual Conference on Smart Structure & NDE 2012*, San Diego, CA/USA, 2012.
14. Z. Guo, K. Kim, G. Lanzara, N. Salowitz, P. Peumans and F.-K. Chang. 2011. "Bio-inspired smart skin based on expandable network", *8th International Workshop on Structural Health Monitoring 2011 – Condition Based Maintenance and Intelligent Structures*, Stanford, CA, USA, 2011.
15. Z. Guo, K. Kim, G. Lanzara, N. Salowitz, P. Peumans and F.-K. Chang. 2011. "Micro-fabricated, expandable temperature sensor network for macro-scale deployment in composite structures", *Proceedings of the 2011 IEEE Aerospace Conference*, Big Sky, Montana, 2011.
16. N. Salowitz, Z. Guo, S.-J. Kim, Y.-H. Li, G. Lanzara and F.-K. Chang. 2013. "Screen-printed piezoceramic actuators/sensors microfabricated on organic films and stretchable networks", *9th International Workshop on Structural Health Monitoring 2013*, Stanford, CA, 2013.
17. Z. Guo. 2014. "Robust Design And Fabrication Of Highly Stretchable Sensor Networks For The Creation Of Intelligent Materials", PhD Thesis, Stanford University, 2014.
18. XFOIL, http://web.mit.edu/drela/Public/web/xfoil/